

## Polyoxometalates

International Edition: DOI: 10.1002/anie.201910491  
German Edition: DOI: 10.1002/ange.201910491Self-Assembly of a Phosphate-Centered Polyoxo-Titanium Cluster:  
Discovery of the Heteroatom Keggin FamilyNing Li<sup>†</sup>, Jiang Liu<sup>†</sup>, Jing-Jing Liu, Long-Zhang Dong, Shun-Li Li, Bao-Xia Dong, Yu-He Kan,  
and Ya-Qian Lan\*

**Abstract:** Over the past 200 years, the most famous and important heteroatom Keggin architecture in polyoxometalates has only been synthesized with Mo, W, V, or Nb. Now, the self-assembly of two phosphate ( $\text{PO}_4^{3-}$ )-centered polyoxo-titanium clusters (PTCs) is presented,  $\text{PTi}_{16}$  and  $\text{PTi}_{12}$ , which display classic heteroatom Keggin and its trivacant structures, respectively. Because  $\text{Ti}^{\text{IV}}$  has lower oxidate state and larger ionic radius than  $\text{Mo}^{\text{VI}}$ ,  $\text{W}^{\text{VI}}$ ,  $\text{V}^{\text{V}}$ , and  $\text{Nb}^{\text{V}}$ , additional  $\text{Ti}^{\text{IV}}$  centres in these PTCs are used to stabilize the resultant heteroatom Keggin structures, as demonstrated by the coresponding theoretical calculation results. These photoactive PTCs can be utilized as efficient photocatalysts for highly selective  $\text{CO}_2$ -to- $\text{HCOOH}$  conversion. This new discovery indicates that the classic heteroatom Keggin family can be assembled with Ti, thus opening a research avenue for the development of PTC chemistry.

Keggin and its lacunary structures constitute the most important and extensive subunit of polyoxometalate (POM) chemistry that features structural diversity and exhibits desirable properties in catalysis, materials science, and energy conversion.<sup>[1]</sup> The archetypical Keggin structure is based on the well-known heteropolyoxometalate cluster having the formula  $[\text{X}_1\text{M}_{12}\text{O}_{40}]^{3-}$  ( $\text{X} = \text{P}, \text{Si}, \text{Ge}, \text{etc.}$ ;  $\text{M} = \text{Mo}^{\text{VI}}, \text{W}^{\text{VI}}$ ), which is made up of four  $\text{M}_3\text{O}_{13}$  units that encapsulate a central heteroatom with a tetrahedral  $\text{XO}_4$  geometry (Supporting Information, Scheme S1). Compared to the original  $\text{Mo}^{\text{VI}}$ - and  $\text{W}^{\text{VI}}$ -based heteroatom Keggin architectures, however, other Keggin analogues (including isopolyoxometalates) composed of metal ions with low accessible oxidation state and large ionic radius need more metal centres ( $>12$ ) to effectively reduce overall cluster charge, and thus a stable molecular cluster.<sup>[2,3]</sup> Besides,

lacunary heteroatom Keggin species, where one or three metal sites are taken off the plenary Keggin structure, also have attracted increasing interest because of their well-defined and highly reactive vacant sites that bring many opportunities for the preparation of multifunctional high-nuclearity clusters and extended frameworks.<sup>[4]</sup>

Despite those advantages mentioned above, the heteroatom Keggin family was only synthesized and developed in  $\text{Mo}^{\text{VI}}$ -,  $\text{W}^{\text{VI}}$ -,  $\text{V}^{\text{V}}$ -, and  $\text{Nb}^{\text{V}}$ -based systems in the past 200 years.<sup>[5]</sup> Considering their fascinating architectures with unexplored functions, development of novel heteroatom Keggin families by other elements has long been an attractive but challenging research field. PTCs are an emerging class of nanoclusters that have achieved the rapid growth in its structure library.<sup>[6]</sup> Because of their intimate structural relationship with POMs,<sup>[7]</sup> they are expected to have great potential to construct more cluster structures as similar as POMs. Nevertheless, the development of PTCs is severely hindered by their daunting synthesis, in which Ti (group 4) ions are prone to fast and spontaneous hydrolysis in hydrous solvents to then generate uncontrolled  $\text{TiO}_2$  precipitation, resulting in a sluggish progress in synthesizing new structures.<sup>[6a]</sup> Although diverse synthetic methods have been largely developed in the past few years,<sup>[8]</sup> there are still very few PTCs that exhibit structural similarity as POMs.<sup>[9]</sup> In particular, the synthesis of famous heteroatom Keggin and its lacunary structures has never been explored in this field, except for very few homo-atom Keggin PTCs.<sup>[10]</sup> Moreover, the homo-atoms in all reported Keggin PTCs are Ti.

Herein,  $\text{Ti}^{\text{IV}}$ -based heteroatom Keggin and its trivacant lacunary architectures,  $[\text{Ti}_{16}(\text{OH})_4\text{O}_{20}(\text{PO}_4)(\text{O}i\text{Pr})_{16}]$ -guests (**PTi<sub>16</sub>**,  $\text{HO}i\text{Pr}$  = isopropanol) and  $[\text{Ti}_{12}\text{O}_{15}(\text{PO}_4)(i\text{PrPO}_4)_3(\text{O}i\text{Pr})_{12}](\text{CHA})_3(\text{H}_2\text{O})$  (**PTi<sub>12</sub>**,  $\text{CHA}$  = cyclohexylammonium), were first structurally synthesized by a facile solvothermal approach, and they can be prepared easily in large scale by increasing reactants ratios. Since the  $\text{Ti}^{\text{IV}}$  has relatively low oxidation state and large ionic radius, additional Ti atoms are used to reduce overall PTC charge for stabilizing the resultant Keggin structures, as demonstrated by density functional theory (DFT) calculations. Additionally, both of these PTCs can be treated as efficient photocatalysts for  $\text{CO}_2$  reduction, and display very high selectivity and activity for  $\text{HCOOH}$  production. Moreover, this is the first report of isolated and soluble PTCs applied in photocatalytic  $\text{CO}_2$  reduction reaction ( $\text{CO}_2\text{RR}$ ).

Crystallographic structural analysis reveals that the **PTi<sub>16</sub>** cluster crystallizes in the cubic space group  $P-43n$  and presents a heteroatom  $\alpha$ -Keggin structure (Figure 1a). As with the classic heteroatom Keggin structure, the central

\*] N. Li,<sup>[†]</sup> Dr. J. Liu,<sup>[†]</sup> J.-J. Liu, L.-Z. Dong, Prof. S.-L. Li, Prof. Y.-Q. Lan  
Jiangsu Collaborative Innovation Centre of Biomedical Functional  
Materials, School of Chemistry and Materials Science  
Nanjing Normal University  
No.1, Wenyuan Road, Nanjing 210023 (China)  
E-mail: yqlan@njnu.edu.cn

N. Li,<sup>[†]</sup> Prof. B.-X. Dong  
School of Chemistry and Chemical Engineering, Yangzhou University  
Yangzhou 225002 (P. R. China)

Prof. Y.-H. Kan  
School of Chemistry and Chemical Engineering Normal University  
Huaian 223300 (P. R. China)

[†] These authors contributed equally to this work.

Supporting information and the ORCID identification number(s) for  
the author(s) of this article can be found under:  
<https://doi.org/10.1002/anie.201910491>.

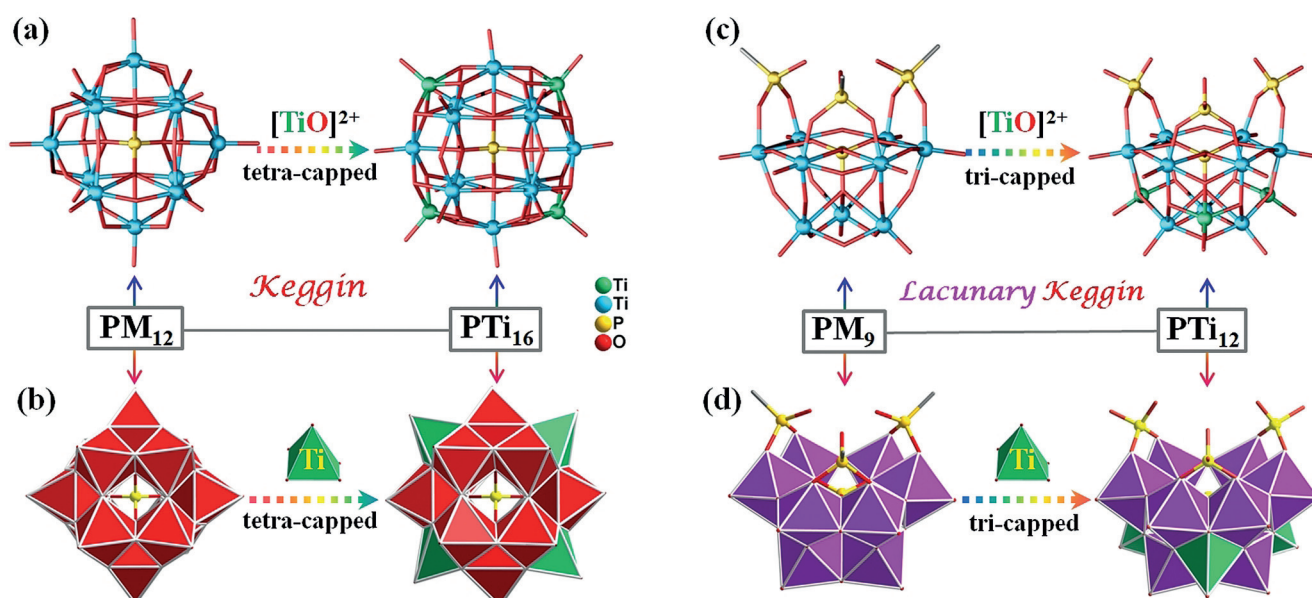


**Figure 1.** The new heteroatom Keggin structures based on PTCs. a),b) Structural and polyhedral relationships between  $\text{PTi}_{16}$  and original heteroatom Keggin structure ( $\text{PM}_{12}$ ,  $\text{M} = \text{Mo}^{\text{VI}}$ ,  $\text{W}^{\text{VI}}$ ). c),d) Structural and polyhedral relationships between  $\text{PTi}_{12}$  and original lacunary heteroatom Keggin structure ( $\text{PM}_9$ ,  $\text{M} = \text{Mo}^{\text{VI}}$ ,  $\text{W}^{\text{VI}}$ ). C, H, and guests are omitted for clarity.

tetrahedron  $\{\text{PO}_4\}$  in  $\text{PTi}_{16}$  connects with twelve Ti atoms to form four triangular and edge-shared  $\{\text{Ti}_3\text{O}_{13}\}$  units by its  $\mu_3\text{-O}$  atoms, and these  $\{\text{Ti}_3\text{O}_{13}\}$  units are corner-linked to the central  $\{\text{PO}_4\}$  (Supporting Information, Figure S1). Moreover, the four square faces between trimetric  $\{\text{Ti}_3\text{O}_{13}\}$  units are capped by four additional  $[\text{TiO}]^{2+}$  units whose five-coordinated Ti centers exhibit distorted square pyramid geometry (Figure 1b; Supporting Information, Figure S1b). The heteroatom  $\alpha$ -Keggin metal-oxo structure of  $\text{PTi}_{16}$  consists of sixteen Ti atoms coordinated to oxo and isopropoxy groups and is encapsulated by sixteen terminal isopropoxy groups. The high formation tendency of spherical  $\text{PTi}_{16}$  is to optimize close-packing of oxygen atoms and minimizes metal-metal repulsion (Supporting Information, Figures S1b, S2a).

By contrast,  $\text{PTi}_{12}$  cluster crystallizes in the orthorhombic space group  $Pbca$  and exhibits an A-type trivacant heteroatom  $\alpha$ -Keggin structure (Supporting Information, Figure S3a) in which three square faces between trimetric  $\{\text{Ti}_3\text{O}_{13}\}$  units are capped by additional three  $[\text{TiO}]^{2+}$  unit (Figure 1c; Supporting Information, Figure S3b). Interestingly, the removed triad (that is, edge-shared  $\{\text{Ti}_3\text{O}_{13}\}$  unit) from the plenary  $\alpha$ -Keggin cluster is replaced by three esterifiable  $\{i\text{PrPO}_4\}$  tetrahedra (Supporting Information, Figure S3), this kind of geometry has been observed in trivacant lacunary polyoxotungstate and -niobate chemistry.<sup>[11]</sup> The central tetrahedron  $\{\text{PO}_4\}$  bonds to nine  $\{\text{TiO}_6\}$  octahedra to form three triangular and edge-shared  $\{\text{Ti}_3\text{O}_{13}\}$  units, which is similar to  $\text{PM}_9$  (Figure 1c,d; Supporting Information, Figure S4). The metal-oxo core of  $\text{PTi}_{12}$  is assembled with twelve Ti atoms, one central  $\{\text{PO}_4\}$ , three  $\mu_2\text{-O}$  and twelve  $\mu_3\text{-O}$  bridges, and is encapsulated by twelve terminal isopropoxy and three esterifiable  $\{\text{PO}_4\}$  groups (Supporting Information, Figure S4). More details about the bond lengths and angles are listed in the Supporting

Information, Table S1. To better understand the structural stability of these two Keggin clusters, we have performed DFT calculations in combination with nucleus independent chemical shifts (NICS), multicenter indices (MCI), and natural bond orbital (NBO) analyses to investigate the electron delocalization. As expected, the calculations indicate that additional four/three  $[\text{TiO}]^{2+}$  units inserted in the  $\text{PTi}_{16}/\text{PTi}_{12}$  structure indeed play a key role in balancing overall PTC charge (see computational details in the Supporting Information).

The phase purity of  $\text{PTi}_{16}$  and  $\text{PTi}_{12}$  was first confirmed by powder X-ray diffraction analysis (Supporting Information, Figure S5). The P element in both PTCs was identified by crystallographic structure, element mapping, X-ray photoelectron spectroscopy (XPS),  $^{31}\text{P}$  solution NMR, and infrared (IR) spectroscopy. As we can see from the element mapping images (Figure 2a–h), O, P, and Ti elements are evenly distributed in two PTCs. The corresponding full-scan spectra of XPS also indicate the existence of above elements including P, and the strong P 2p peak at 133.6/133.2 eV can be assigned to the characteristic of P–O bond (Figure 2i,k; Supporting Information, Figure S6). Meanwhile, the high-resolution Ti 2p spectra for  $\text{PTi}_{16}$  and  $\text{PTi}_{12}$  clearly exhibit two regions of Ti 2p<sub>1/2</sub> (ca. 464.4 eV) and Ti 2p<sub>3/2</sub> (ca. 458.6 eV) with about 5.8 eV binding energy difference, being indicative of the sole presence of typical  $\text{Ti}^{4+}$  (Figure 2j,l). Besides, the liquid-state  $^{31}\text{P}$  NMR spectra of  $\text{PTi}_{16}$  and  $\text{PTi}_{12}$  also agree with the structures determined by single crystal X-ray diffraction (Supporting Information, Figure S7). For  $\text{PTi}_{16}$ , the spectrum only has one phosphate peak at  $\delta = +2.74$  ppm that corresponds to the central  $\{\text{PO}_4\}$  group in  $\alpha$ -Keggin structure. No other  $^{31}\text{P}$  NMR resonances were detected, indicating that there are no impurities or any minor phases containing phosphorus. The spectrum of  $\text{PTi}_{12}$  features two

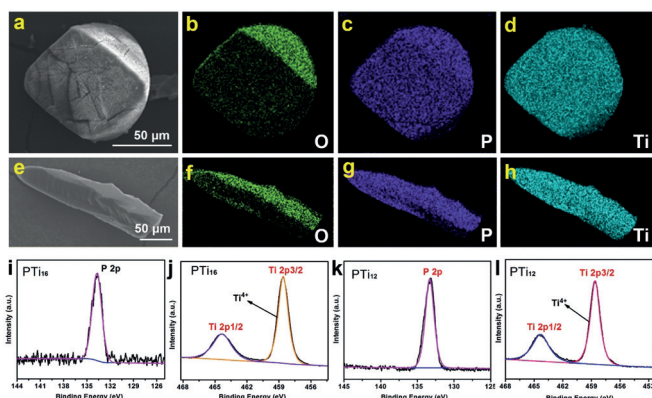


**Figure 2.** The morphology, elemental distribution, and XPS of **PTi<sub>16</sub>** and **PTi<sub>12</sub>**. a)–d) The SEM image and elemental mapping of **PTi<sub>16</sub>**. e)–h) The SEM image and elemental mapping of **PTi<sub>12</sub>**. The XPS high-resolution scans of P 2p and Ti 2p for **PTi<sub>16</sub>** (i,j) and **PTi<sub>12</sub>** (k,l).

phosphate resonances in a 3:1 ratio (integral peak areas ratio), which are assigned to three esterifiable {iPrPO<sub>4</sub>} and one central {PO<sub>4</sub>} groups in trivacant Keggin structure stoichiometry. IR spectra were further used to identify fingerprint peaks of multiple P–O bands from different {PO<sub>4</sub>} groups (Supporting Information, Figure S8). The two peaks at about 1067 and about 1005 cm<sup>−1</sup> are assigned to esterifiable and central {PO<sub>4</sub>} groups, respectively, which are very similar to infrared studies on other PO<sub>4</sub>-centered Keggin and lacunary derivatives.<sup>[11a,12]</sup> The liquid-state UV/Vis absorption spectra also display the characteristic of Keggin-type structures (Supporting Information, Figure S9). Additionally, **PTi<sub>16</sub>** and **PTi<sub>12</sub>** clusters have good solubility in conventional organic solvents and aqueous phase, which can be demonstrated by electrospray ionization mass spectrometry (ESI-MS) analysis (Figure 3; Supporting Information, Figure S10). Thermogravimetric analysis (TGA) was further performed on their polycrystalline samples under N<sub>2</sub> atmos-

phere to investigate their thermal stability (Supporting Information, Figure S11).

It is well-recognized that titanium containing semiconductors and solids can efficiently photocatalytic reduce CO<sub>2</sub> into value-added chemicals.<sup>[13]</sup> However, the reports on titanium-oxo clusters as photocatalysts for CO<sub>2</sub> reduction are scarce, except for a few titanium-based MOFs.<sup>[14]</sup> Both of **PTi<sub>16</sub>** and **PTi<sub>12</sub>** display strong absorption in the ultraviolet region, from which the band gaps (*E<sub>g</sub>*) can be determined to be 2.80 and 2.85 eV, respectively, indicating that they also display semiconductor-like properties (Figure 4a,b). A cyclic

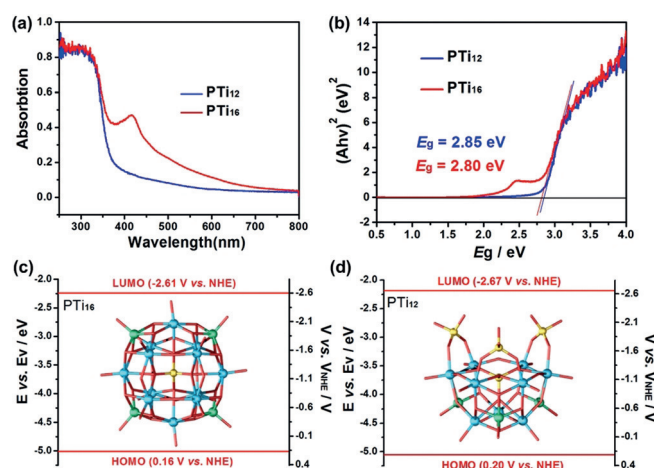


**Figure 4.** a) UV/Vis spectra, b) Tauc plots, and c,d) band structure diagrams (including LUMO and HOMO levels) for **PTi<sub>16</sub>** and **PTi<sub>12</sub>**.

voltammetry (CV) test and ultraviolet photoelectron spectroscopy (UPS) were performed to determine the LUMO and HOMO levels of **PTi<sub>16</sub>** and **PTi<sub>12</sub>** (Supporting Information, Figures S12, S13). Moreover, the HOMO and LUMO energies determined by CVs are very close to that of optical Tauc plots associated with UPS, and they were converted to electrochemical energy potentials in volts vs. normal hydrogen electrode (NHE) (Figure 4c,d). It is obvious that the LUMO positions of **PTi<sub>16</sub>** and **PTi<sub>12</sub>** are more negative than the reduction potentials of many photocatalytic products. We thus conducted UV-light-driven photocatalytic reduction of CO<sub>2</sub> over **PTi<sub>16</sub>** and **PTi<sub>12</sub>**, with triethanolamine (TEOA) and CH<sub>3</sub>CN as electron donor and solvent, respectively, which can promote CO<sub>2</sub> solubility and photo-generated electron transfer.<sup>[15]</sup> During the photoreaction process, HCOOH is the only liquid product detected by ion chromatography (IC; Supporting Information, Figure S14), while other gaseous products including competitive H<sub>2</sub>, CO, and CH<sub>4</sub> are also observed by gas chromatography (GC; Supporting Information, Figure S15). From Figure 5a, the production of HCOOH for both titanium-oxo clusters has a continuous growth as the irradiation time increases. After 18 h, the produced HCOOH for **PTi<sub>16</sub>** reaches up to 24.13 μmol (268.12 μmol g<sup>−1</sup> h<sup>−1</sup>), which is comparable to other reported titanium-containing semiconductors and MOF materials.<sup>[14,16]</sup> By contrast, **PTi<sub>12</sub>** shows a relatively low HCOOH production of 9.21 μmol (122.80 μmol g<sup>−1</sup> h<sup>−1</sup>) after 15 hours. With the extended irrita-

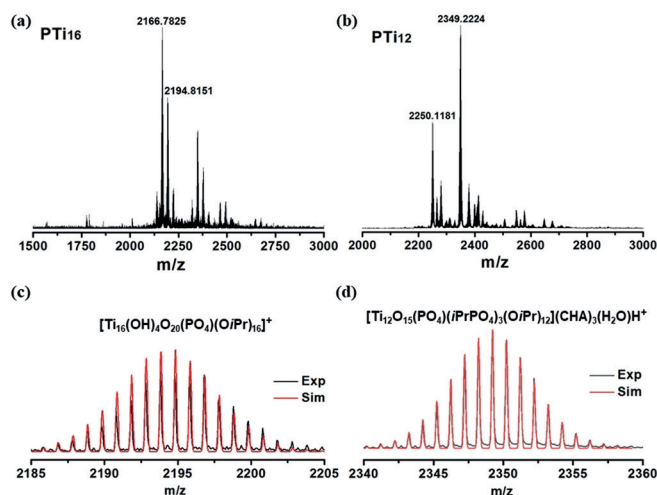


**Figure 3.** Enlarged *m/z* range of positive-mode ESI-MS spectra of a) **PTi<sub>16</sub>** and b) **PTi<sub>12</sub>** dissolved in acetonitrile solution. Experimental (black line) and simulated (red line) HRESI-MS spectra of **PTi<sub>16</sub>** (c, *m/z* 2194.8151) and **PTi<sub>12</sub>** (d, *m/z* 2349.2224).



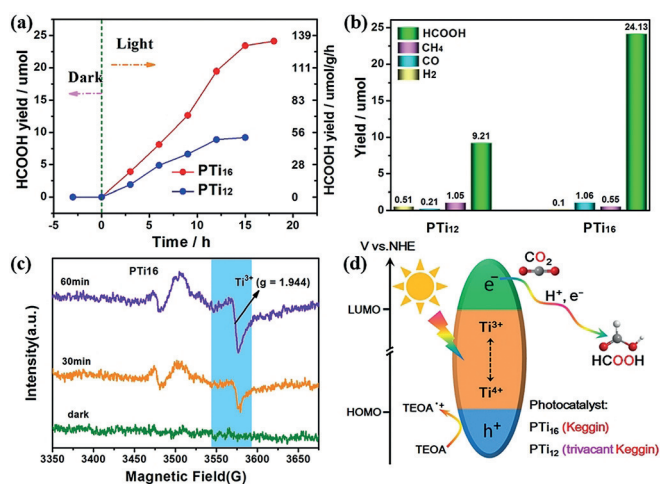


**Figure 5.** Photocatalytic characterizations over **PTi<sub>16</sub>** and **PTi<sub>12</sub>**.

a) Amounts of HCOOH produced as a function of the time of UV light irradiation. b) The yield distribution of different photocatalytic products. c) ESR spectra of **PTi<sub>16</sub>**. d) The proposed reaction mechanism.

tion time, the production of gaseous products ( $\text{H}_2$ ,  $\text{CO}$ , and  $\text{CH}_4$ ) also has a growth trend but low total yield, resulting in that very high selectivity for  $\text{CO}_2$ -to- $\text{HCOOH}$  photosynthesis was obtained by **PTi<sub>16</sub>** (93.4%) and **PTi<sub>12</sub>** (83.9%) (Figure 5b). Moreover, this is the first report of titanium-oxo cluster system applied to the  $\text{CO}_2$  photoreduction. To confirm the photocatalytic activity of **PTi<sub>16</sub>** and **PTi<sub>12</sub>**, a series of deletional control experiments were carried out in the absence of photocatalysts,  $\text{CO}_2$ , TEOA, or UV-light illumination. Results revealed that no products can be detected by IC and GC (Supporting Information, Table S2), corroborating the photocatalytic potential of these titanium-oxo clusters for reducing  $\text{CO}_2$  into HCOOH. The UV/Vis absorption spectra after photocatalytic reaction still displayed Keggin-based character (Supporting Information, Figure S16), which excludes the influence of the decomposed active components from catalysts on the photocatalytic activity. Additionally, nearly unchanged  $^{31}\text{P}$  NMR spectra and ESI-MS after reaction also prove the structural stability of **PTi<sub>16</sub>** and **PTi<sub>12</sub>** (Supporting Information, Figures S17, S18). The isotopic  $^{13}\text{CO}_2$  experiment was conducted under identical photocatalytic reaction condition to investigate the carbon source origin of the produced HCOOH, and the resultant reaction filtrate was characterized by  $^{13}\text{C}$  NMR spectroscopy. As shown in the Supporting Information, Figure S19, the  $^{13}\text{C}$  NMR spectrum gives a clear signal at 164.3 ppm, corresponding to  $\text{HCOO}^-$ , which is in line with that demonstrated in other important works.<sup>[14,17]</sup> Also, this  $\text{HCOO}^-$  signal cannot be observed when using  $^{12}\text{CO}_2$  instead of  $^{13}\text{CO}_2$ , except for additional peaks corresponding to  $\text{CD}_3\text{CN}$  and TEOA (Supporting Information, Figure S20). These results unambiguously confirm that the produced  $\text{HCOO}^-$  indeed originates from  $\text{CO}_2$ , suggesting that both titanium-oxo clusters are very active and capable of reducing  $\text{CO}_2$  to  $\text{HCOO}^-$  under UV light irradiation. Electron spin resonance (ESR) measurements were further conducted to study the mechanism behind the  $\text{CO}_2$  photoreduction over **PTi<sub>16</sub>** and **PTi<sub>12</sub>**. As shown in

Figure 5c and the Supporting Information, Figure S21, the original reaction systems including photocatalyst and TEOA in the dark under  $\text{N}_2$  atmosphere did not show any ESR signal. When the reaction systems were irradiated by UV light under identical condition, a clear signal of  $\text{Ti}^{3+}$  ( $g = 1.944$ ) can be observed from their ESR spectra. This means that the  $\text{Ti}^{4+}$  within titanium-oxo clusters were reduced into  $\text{Ti}^{3+}$  by receiving photoexcited electrons transferred from  $\text{O}^{2-}$ , while the corresponding photo-generated holes were quenched by TEOA. Moreover, the intensity of  $\text{Ti}^{3+}$  signal increased with the extended irradiation time. When the reaction system was contacted with  $\text{CO}_2$  or  $\text{O}_2$  atmosphere, the ESR signal of  $\text{Ti}^{3+}$  disappeared, indicating that the photogenerated  $\text{Ti}^{3+}$  is involved in  $\text{CO}_2$  reduction reaction. The ESR results reveal that the  $\text{Ti}^{4+}$  atoms within **PTi<sub>16</sub>** and **PTi<sub>12</sub>** are the photocatalytic active sites for the  $\text{CO}_2$ -to- $\text{HCOOH}$  reduction, and are in accordance with that in titanium-based MOFs.<sup>[14,18]</sup>

Based on the above analysis, the mechanism for the photocatalytic  $\text{CO}_2$  reduction can be illustrated as shown in Figure 5d. Upon UV light irradiation, an excited charge separation state (the generation of electrons and holes) occurs in titanium-oxo cluster by transferring a photogenerated electron from  $\text{O}^{2-}$  to  $\text{Ti}^{4+}$ .  $\text{Ti}^{4+}$  is thus reduced to  $\text{Ti}^{3+}$  whereas TEOA acts as an electron donor to consume the produced hole. Subsequently, the  $\text{Ti}^{3+}$  donates one photogenerated electron to the absorbed  $\text{CO}_2$  for HCOOH production and goes back to  $\text{Ti}^{4+}$ . By this way, a complete photocatalytic cycle of  $\text{CO}_2$ -to- $\text{HCOOH}$  reduction can be achieved by  $\text{Ti}^{3+}$  in the presence of TEOA as electron and hydrogen donors.

In summary, a new heteroatom Keggin family based on PTCs has been synthesized. The DFT calculation results reveal that the capped  $[\text{TiO}]^{2+}$  units play a key role in stabilizing the resultant Keggin clusters. Moreover, these soluble PTCs display high selectivity and activity for  $\text{CO}_2$ -to- $\text{HCOOH}$  photoconversion. It is predicted that this discovery will not only enrich the heteroatom Keggin family but also open a new research direction for the development and application of novel PTC materials.

## Acknowledgements

This work was financially supported by NSFC (No. 21622104, 21871141, 21871142, 21701085, and 21901122); the NSF of Jiangsu Province of China (No. BK20171032); the Natural Science Research of Jiangsu Higher Education Institutions of China (No. 17KJB150025 and 19KJB150011) and Project funded by China Postdoctoral Science Foundation (No. 2018M630572 and 2019M651873). We thank the staff from BL17B beamline of National Facility for Protein Science Shanghai (NFPS) at Shanghai Synchrotron Radiation Facility for assistance during data collection.

## Conflict of interest

The authors declare no conflict of interest.

**Keywords:** CO<sub>2</sub> photoreduction · Keggin structures · polyoxo-titanium cluster

**How to cite:** *Angew. Chem. Int. Ed.* **2019**, *58*, 17260–17264  
*Angew. Chem.* **2019**, *131*, 17420–17424

- [1] a) H. N. Miras, J. Yan, D.-L. Long, L. Cronin, *Chem. Soc. Rev.* **2012**, *41*, 7403–7430; b) S.-S. Wang, G.-Y. Yang, *Chem. Rev.* **2015**, *115*, 4893–4962.
- [2] A. Bino, M. Ardon, D. Lee, B. Spingler, S. J. Lippard, *J. Am. Chem. Soc.* **2002**, *124*, 4578–4579.
- [3] a) M. Grabau, J. Forster, K. Heussner, C. Streb, *Eur. J. Inorg. Chem.* **2011**, 1719–1724; b) O. Sadeghi, L. N. Zakharov, M. Nyman, *Science* **2015**, *347*, 1359–1362; c) G. N. Newton, S. Yamashita, K. Hasumi, J. Matsuno, N. Yoshida, M. Nihei, T. Shiga, M. Nakano, H. Nojiri, W. Wernsdorfer, H. Oshio, *Angew. Chem. Int. Ed.* **2011**, *50*, 5716–5720; *Angew. Chem.* **2011**, *123*, 5834–5838.
- [4] a) B.-J. Yan, X.-S. Du, R.-W. Huang, J.-S. Yang, Z.-Y. Wang, S.-Q. Zang, T. C. W. Mak, *Inorg. Chem.* **2018**, *57*, 4828–4832; b) C. Li, N. Mizuno, K. Yamaguchi, K. Suzuki, *J. Am. Chem. Soc.* **2019**, *141*, 7687–7692.
- [5] a) J. F. Keggin, *Nature* **1933**, *131*, 908; b) A. Müller, F. Peters, M. T. Pope, D. Gatteschi, *Chem. Rev.* **1998**, *98*, 239–272; c) M. Nyman, F. Bonhomme, T. M. Alam, M. A. Rodriguez, B. R. Cherry, J. L. Krumhansl, T. M. Nenoff, A. M. Sattler, *Science* **2002**, *297*, 996–998; d) R. Kato, A. Kobayashi, Y. Sasaki, *J. Am. Chem. Soc.* **1980**, *102*, 6571–6572; e) J.-H. Son, W. H. Casey, *Chem. Commun.* **2015**, *51*, 1436–1438.
- [6] a) W. H. Fang, L. Zhang, J. Zhang, *Chem. Soc. Rev.* **2018**, *47*, 404–421; b) P. Coppens, Y. Chen, E. Trzop, *Chem. Rev.* **2014**, *114*, 9645–9661.
- [7] L. Rozes, C. Sanchez, *Chem. Soc. Rev.* **2011**, *40*, 1006–1030.
- [8] a) W.-H. Fang, L. Zhang, J. Zhang, *J. Am. Chem. Soc.* **2016**, *138*, 7480–7483; b) G. Zhang, C. Liu, D.-L. Long, L. Cronin, C.-H. Tung, Y. Wang, *J. Am. Chem. Soc.* **2016**, *138*, 11097–11100.
- [9] a) G. Zhang, J. Hou, M. Li, C.-H. Tung, Y. Wang, *Inorg. Chem.* **2016**, *55*, 4704–4709; b) N. Steunou, G. Kickelbick, K. Boubekeur, C. Sanchez, *J. Chem. Soc. Dalton Trans.* **1999**, 3653–3655.
- [10] a) J. D. Sokolow, E. Trzop, Y. Chen, J. Tang, L. J. Allen, R. H. Crabtree, J. B. Benedict, P. Coppens, *J. Am. Chem. Soc.* **2012**, *134*, 11695–11700; b) C. F. Campana, Y. Chen, V. W. Day, W. G. Klemperer, R. A. Sparks, *J. Chem. Soc. Dalton Trans.* **1996**, 691–702; c) S. Chen, W.-H. Fang, L. Zhang, J. Zhang, *Inorg. Chem.* **2018**, *57*, 8850–8856.
- [11] a) M. Nyman, A. J. Celestian, J. B. Parise, G. P. Holland, T. M. Alam, *Inorg. Chem.* **2006**, *45*, 1043–1052; b) A. Mazeaud, N. Ammari, F. Robert, R. Thouvenot, *Angew. Chem. Int. Ed. Engl.* **1996**, *35*, 1961–1964; *Angew. Chem.* **1996**, *108*, 2089–2091.
- [12] J.-H. Son, W. H. Casey, *Chem. Commun.* **2015**, *51*, 12744–12747.
- [13] A. Dhakshinamoorthy, S. Navalón, A. Corma, H. Garcia, *Energy Environ. Sci.* **2012**, *5*, 9217–9233.
- [14] Y. Fu, D. Sun, Y. Chen, R. Huang, Z. Ding, X. Fu, Z. Li, *Angew. Chem. Int. Ed.* **2012**, *51*, 3364–3367; *Angew. Chem.* **2012**, *124*, 3420–3423.
- [15] S. Wang, W. Yao, J. Lin, Z. Ding, X. Wang, *Angew. Chem. Int. Ed.* **2014**, *53*, 1034–1038; *Angew. Chem.* **2014**, *126*, 1052–1056.
- [16] K. Li, B. Peng, T. Peng, *ACS Catal.* **2016**, *6*, 7485–7527.
- [17] a) H.-Q. Xu, J. Hu, D. Wang, Z. Li, Q. Zhang, Y. Luo, S.-H. Yu, H.-L. Jiang, *J. Am. Chem. Soc.* **2015**, *137*, 13440–13443; b) N. Li, J. Liu, J. J. Liu, L. Z. Dong, Z. F. Xin, Y. L. Teng, Y. Q. Lan, *Angew. Chem. Int. Ed.* **2019**, *58*, 5226–5231; *Angew. Chem.* **2019**, *131*, 5280–5285.
- [18] M. Dan-Hardi, C. Serre, T. Frot, L. Rozes, G. Maurin, C. Sanchez, G. Férey, *J. Am. Chem. Soc.* **2009**, *131*, 10857–10859.

Manuscript received: August 16, 2019

Accepted manuscript online: September 26, 2019

Version of record online: October 16, 2019